

Rotating black holes in a class of scalar-Gauss-Bonnet gravity

Shoupan Liu,^{1,*} Yunqi Liu,^{1,†} Yan Peng,^{2,‡} and Cheng-Yong Zhang^{3,§}

¹*Center for Gravitation and Cosmology,
College of Physical Science and Technology,
Yangzhou University, Yangzhou 225009, China*

²*School of Mathematical Sciences, Qufu Normal University, Qufu, Shandong 273165, China*

³*Department of Physics and Siyuan Laboratory,
Jinan University, Guangzhou 510632, China*

Abstract

In this study, we investigate rotating black hole solutions within a scalar–Gauss–Bonnet gravity framework that incorporates a quadratic Gauss–Bonnet term. By employing a quadratic–exponential coupling function between the scalar field and the Gauss–Bonnet invariant, we derive both the standard General Relativity solutions and novel scalarized black hole configurations. Utilizing a pseudo-spectral method to solve the coupled field equations, we examine how black hole spin and coupling constants influence the existence and properties of these solutions. Our findings reveal that both the rotation of the black hole and the quadratic coupling term effectively constrain the parameter space available for scalarization. Moreover, we demonstrate that, over a wide range of parameters, scalarized black holes exhibit higher entropy than Kerr black holes of equivalent mass and spin, indicating that they are thermodynamically favored. These results significantly expand the phase space of black holes in modified gravity theories.

* shoupan_liu@163.com

† yunqiliu@yzu.edu.cn (corresponding author)

‡ yanpengphy@163.com

§ zhangcy@email.jnu.edu.cn

I. INTRODUCTION

In general relativity (GR), stationary vacuum black holes (BHs) are uniquely described by the Kerr metric [1] and are therefore fully characterized by their mass, electric charge, and angular momentum [2]. This remarkable simplicity is encapsulated in the “no-hair” conjecture [3–5] and the Kerr hypothesis [6], both of which have long been cornerstones of GR. Moreover, the no-hair conjecture has been extended to alternative theories, such as Brans-Dicke theories, certain classes of scalar-tensor theories, and Gallilen models of gravity [7–9].

Over the past decades, however, a growing body of work in modified gravity theories has revealed the existence of “hairy” BH solutions that carry additional charges beyond the traditional parameters [10–13]. Notable examples include black holes in the presence of Yang-Mills fields [14–17], Skyrme [18, 19], conformally coupled scalar fields [20], and dilatonic or colored BHs within Einstein-dilaton-Gauss-Bonnet theory [21–25]. Other cases involve rotating [26–28] or shift-symmetric Galileon hairy BHs [29, 30]. Recent studies have provided significant insights into the phase diagram of gravitational systems beyond GR [31–41]. This is particularly interesting in theories that may be affected by tachyonic instability [11, 32, 42–44], which can trigger *spontaneous scalarization*. This mechanism often appears in models where a real scalar field is non-minimally coupled to specific source terms. The presence of non-minimal coupling acts as an effective mass squared term in the scalar field’s equation of motion; when this effective mass squared term becomes negative, a tachyonic instability may ensue. Such source terms could include geometrically invariant quantities, such as the Gauss-Bonnet invariant in extended scalar-Gauss-Bonnet (sGB) theory [45–53], the Ricci scalar for non-conformally invariant BHs [54], the Chern-Simons invariant [55], or the Maxwell invariant $F_{\mu\nu}F^{\mu\nu}$ [56, 57]. Depending on the form of the coupling function, the onset of scalarization may follow a linear or a nonlinear route, the latter is often referred to as nonlinear scalarization [33, 38, 58–62].

Generally, scalarization is unattainable for BHs with intermediate and supermassive mass scales [31–36]. Consequently, the prevailing expectation is that BHs in these mass ranges should be well described by the Kerr metric, even when solar-mass BHs are not. However, Ref. [63] considers a model in which the Gauss-Bonnet term is quadratically coupled to a scalar field. By studying the model in spherical symmetry, they found that unlike in the conventional framework, BHs can undergo spontaneous scalarization within a finite mass window, which may include supermassive BHs. Such deviations are particularly interesting because they offer a potential observation window through future gravitational wave detectors like LISA, Taiji, and TianQin to probe into the underlying gravitational theory [64–67].

In the present paper, we extend these investigations to rotating BHs. By employing a quadratic-exponential coupling function, we explore how the inclusion of a quadratic Gauss-Bonnet term modifies the spectrum of rotating BH solutions. Our study addresses two central questions: How does the presence of angular momentum affect the onset and domain of scalarization? And how do quadratic curvature corrections influence the stability and thermodynamic properties of these scalarized configurations compared to their Kerr counterparts? To answer these questions, we numerically solve the full set of modified field equations under stationary and axisymmetric assumptions using the Chebyshev pseudo-spectral method combined with a Newton-Raphson iterative scheme. Our analysis reveals that both the spin parameter and the additional quadratic coupling act to suppress the scalarization, thereby reducing the parameter space in which scalarized solutions exist. Nevertheless, in many regimes the scalarized BHs exhibit higher entropy than Kerr BHs of the same mass and spin, suggesting that they are thermodynamically favored.

The paper is organized as follows. Sec. II establishes the theoretical framework including ac-

tion, field equations, and numerical boundary conditions. We further analyze the stability of general relativistic black holes under scalar perturbations and discuss the mechanisms of sGB coupling that drive spontaneous. Sec.III details the numerical methodology employed to solve the system, focusing on the Chebyshev pseudo-spectral approach and the treatment of boundary conditions in compactified radial coordinates. Numerical results are presented in Sec.IV, where we systematically explore the parameter space to characterize scalarized black hole solutions and their dependence on spin, coupling constants. Finally, Sec.V summarizes our conclusions. Throughout this work, we adopt units $G = c = 1$.

II. THEORETICAL SETUP

A. Action and basic equations

We consider a four-dimensional sGB gravity theory with quadratic curvature corrections, defined by the action [63]:

$$S = \frac{1}{16\pi} \int d^4x \sqrt{-g} [R - (\partial\phi)^2 + \alpha_1 F(\phi)\mathcal{G} - 2\alpha_2^3 F(\phi)(\psi\mathcal{G} - \frac{\psi^2}{2})], \quad (1)$$

where the Gauss-Bonnet invariant is

$$\mathcal{G} = R^2 - 4R_{\alpha\beta}R^{\alpha\beta} + R_{\alpha\beta\gamma\sigma}R^{\alpha\beta\gamma\sigma}, \quad (2)$$

with R , $R_{\alpha\beta}$ and $R_{\alpha\beta\gamma\sigma}$ denoting the Ricci scalar, Ricci tensor, and Riemann tensor respectively. The theory contains two dimensionless coupling constants α_1 and α_2 (with dimensions of length squared), a dimensionless real scalar field ϕ , and an auxiliary field ψ with dimensions inverse length to the fourth, which is the same as \mathcal{G} .

Varying the action with respect to the metric yields the Einstein field equations:

$$\mathcal{E}_{\mu\nu} = G_{\mu\nu} - T_{\mu\nu} = 0, \quad (3)$$

where the effective energy-momentum tensor contains contributions from both scalar fields and curvature couplings:

$$T_{\mu\nu} = \nabla_\mu\phi\nabla_\nu\phi - \frac{1}{2}g_{\mu\nu}[(\nabla\phi)^2 + \alpha_2^3\psi^2 F(\phi)] + 4P_{\mu\alpha\nu\beta}\nabla^\alpha\nabla^\beta[(\alpha_1 - 2\alpha_2^3\psi)F(\phi)], \quad (4)$$

with the double dual Riemann tensor

$$P_{\mu\nu\alpha\beta} \equiv \frac{1}{4}\epsilon_{\mu\nu\gamma\delta}R^{\rho\sigma\gamma\delta}\epsilon_{\rho\sigma\alpha\beta} = R_{\mu\nu\alpha\beta} + 2g_{\mu[\beta}R_{\alpha]\nu} + 2g_{\nu[\alpha}R_{\beta]\mu} + Rg_{\mu[\alpha}g_{\beta]\nu}. \quad (5)$$

The scalar field equations follow from variation with respect to ϕ :

$$\square\phi + \left[\alpha_1\mathcal{G} - 2\alpha_2^3\left(\psi\mathcal{G} - \frac{\psi^2}{2}\right) \right] \frac{F'(\phi)}{2} = 0, \quad (6)$$

where the prime “'” denotes the derivative with respect to scalar field ϕ . The scalar ψ acts as a Lagrange multiplier, which is not dynamical and satisfies the following equation

$$\psi - \mathcal{G} = 0. \quad (7)$$

From Eq.(7), one can see that actually the action (1) includes a term of \mathcal{G}^2 .

In this paper, we will consider a quadratic-exponential coupling $F(\phi) = \frac{1}{\kappa}(1 - e^{-\kappa\phi^2})$ to study the properties of scalarized solutions where κ is a constant. The coupling function has a stationary point that satisfies $F(\phi) = 0$, $F'(\phi) = 0$. By the properties of the coupling function, it is easy to find that the equations of motion, Eqs.(3) and (6), allow the GR solutions. For convenience, we set $\phi = 0$ at the stationary point. However, the GR configuration may be unstable for some model parameters. To show the instability of GR BHs and the potential scalarization, we turn to the linear perturbation analysis. By linearizing Eq.(6) around $\phi = 0$, we obtain the equation of motion governing the scalar perturbation ϕ_p as follows

$$\square\phi_p = m_{eff}^2\phi_p, \quad m_{eff}^2 = -\frac{1}{2}(\alpha_1\mathcal{G} - \alpha_2^3\mathcal{G}^2)F''(0) \quad (8)$$

where we have substituted the equation of motion Eq.(7) into Eq.(6), m_{eff}^2 is the effective mass squared of the perturbation. The different behavior of the derivative $F''(0)$ leads to a different scalarization mechanism. For the quadratic-exponential coupling in this work, we have the value $F''(0) \neq 0$ which means the squared effective mass would be negative enough that make the perturbations tachyonically unstable [32, 68–72], as a result the GR BH solution would be unstable and undergo spontaneous scalarization.

B. Equations of motion and boundary behaviors

To construct stationary axisymmetric solutions, we adopt a quasi-isotropic coordinate system with metric Ansatz [73] :

$$ds^2 = -f\mathcal{N}^2 dt^2 + \frac{g}{f} \left[h(dr^2 + r^2 d\theta^2) + r^2 \sin^2\theta \left(d\varphi - \frac{W}{r}(1 - \mathcal{N})dt \right)^2 \right], \quad (9)$$

where $\mathcal{N} = 1 - r_H/r$ regularizes the horizon at $r = r_H$, and the dimensionless functions f , g , h , and W depend on the radial r and the angular parameter θ .

To solve the system, we employ the following equations that diagonalize the Einstein tensor with respect to the differential operator $\partial_r^2 + r^{-2}\partial_\theta^2$,

$$0 = -\mathcal{E}_\mu^\mu + 2\mathcal{E}_t^t + \frac{2Wr_H}{r^2}\mathcal{E}_t^\varphi, \quad (10a)$$

$$0 = \mathcal{E}_t^\varphi, \quad (10b)$$

$$0 = \mathcal{E}_r^r + \mathcal{E}_\theta^\theta, \quad (10c)$$

$$0 = \mathcal{E}_\varphi^\varphi - \frac{Wr_H}{r^2}\mathcal{E}_t^\varphi - \mathcal{E}_r^r - \mathcal{E}_\theta^\theta \quad (10d)$$

Asymptotic flatness imposes boundary conditions at spatial infinity ($r \rightarrow \infty$) : $\lim_{r \rightarrow \infty} f = \lim_{r \rightarrow \infty} g = \lim_{r \rightarrow \infty} h = 1$, $\lim_{r \rightarrow \infty} 2r_H r^2 \partial_r W + (2r_H + r^2 \partial_r f)^2 \chi = 0$ with $\chi \equiv J/M^2$ defining the dimensionless spin parameter, and $\lim_{r \rightarrow \infty} \phi = \lim_{r \rightarrow \infty} \psi = 0$. Axial symmetry and regularity require vanishing angular derivatives at the symmetry axis $\theta = 0, \pi$: $\partial_\theta f = \partial_\theta g = \partial_\theta h = \partial_\theta W = \partial_\theta \phi = \partial_\theta \psi = 0$. Furthermore, the absence of conical singularities imposes that on the symmetry axis: $h = 1$ for $\theta = 0, \pi$.

The event horizon boundary conditions are $f - r_H \partial_r f|_{r=r_H} = g + r_H \partial_r g|_{r=r_H} = \partial_r h|_{r=r_H} = W + r_H \partial_r W/2|_{r=r_H} = 0$.

Most of the physical quantities of interest are encapsulated in the metric functions evaluated either at the horizon or at infinity. Starting with the asymptotic quantities, the Arnowitt-Deser-Misner (ADM) mass M and the angular momentum J can be extracted from the asymptotic expansion:

$$\begin{aligned} g_{tt} &= -f\mathcal{N}^2 + \frac{g(1-\mathcal{N})^2 W^2}{f} \sin^2 \theta = -1 + \frac{2M}{r} + \mathcal{O}(r^{-2}), \\ g_{t\varphi} &= -\frac{gr(1-\mathcal{N})W}{f} \sin^2 \theta = -\frac{2J}{r} \sin^2 \theta + \mathcal{O}(r^{-2}). \end{aligned} \quad (11)$$

Scalar charge Q_s appears in the far-field behavior:

$$\phi = \frac{Q_s}{r} + \mathcal{O}(r^{-2}). \quad (12)$$

For numerical implementation of the Einstein-scalar system via the Chebyshev pseudo-spectral method, we introduce compactified radial coordinate $x = 1 - 2r_H/r$ that map the semi-infinite domain $r \in [r_H, \infty)$ to a finite interval $x \in [-1, 1]$. This coordinate transformation regularizes the event horizon at $x = -1$ while preserving asymptotic flatness at $x = 1$. Then the BH mass becomes

$$M = r_H (1 + \partial_x f)|_{x=1}. \quad (13)$$

The horizon geometry is encoded in the induced metric:

$$d\Sigma^2 = \gamma_{ij} dx^i dx^j = \frac{r_H^2 g}{f} [h d\theta^2 + \sin^2 \theta d\varphi^2] \Big|_{x=-1}, \quad (14)$$

which allows computation of black hole entropy via the Iyer-Wald formalism [74, 75]

$$S = \frac{A_H}{4} + \frac{1}{4} \int_{\mathcal{H}} d^2x \sqrt{\gamma} (\alpha_1 - 2\alpha_2^3 \psi) F(\phi) \widetilde{R}, \quad (15)$$

where \mathcal{H} denotes the horizon, γ is the determinant of the induced metric and \widetilde{R} is the Ricci scalar on it. The horizon area A_H is explicitly given by

$$A_H = 2\pi r_H^2 \int_0^\pi d\theta \sin \theta \frac{g \sqrt{h}}{f} \Big|_{x=-1}. \quad (16)$$

III. NUMERICAL METHOD

In this section, we give a brief description of the numerical methods. We implement the Chebyshev pseudo-spectral method in conjunction with the Newton-Raphson method to solve the coupled system governed by Eqs.(6), (7) and (10). This method has been widely employed in studying rotating black hole solutions [73].

In the compactified coordinate, the boundary conditions at horizon $x = -1$ take the following form:

$$\begin{aligned} f - 2\partial_x f &= 0, & g + 2\partial_x g &= 0, & \partial_x h &= 0, \\ W - \partial_x W &= 0, & \partial_x \phi &= \partial_x \psi &= 0. \end{aligned} \quad (17)$$

The asymptotic boundary conditions at spatial infinity ($x = 1$) can be written as

$$f = g = h = 1, \quad \partial_x W + \chi(1 + \partial_x f)^2 = 0 \quad \text{and} \quad \phi = \psi = 0. \quad (18)$$

Exploiting equatorial reflection symmetry ($\theta \rightarrow \pi - \theta$), we restrict the angular domain to $\theta \in [0, \pi/2]$ and construct spectral expansions for the six functions $\mathcal{F}^{(k)} = \{f, g, h, W, \phi, \psi\}$ using tensor products of Chebyshev polynomials and cosine basis functions:

$$\mathcal{F}^{(k)}(x, \theta) = \sum_{i=0}^{N_x-1} \sum_{j=0}^{N_\theta-1} \alpha_{ij}^{(k)} T_i(x) \cos(2j\theta), \quad (19)$$

where $T_i(x) = \cos(i \arccos x)$ denotes the i -th Chebyshev polynomial, $\alpha_{ij}^{(k)}$ represent spectral coefficients, and N_x and N_θ are the resolutions in the radial and angular directions. In this paper, we mainly use resolutions of $N_x = 40$ and $N_\theta = 8$ for the computations, with convergence details provided in Appendix.

Substituting the metric Ansatz (9) into the field equations (6),(7) and (10) generates a system of nonlinear partial differential equations containing the functions and their first and second derivatives ($\mathcal{F}^{(k)}, \partial_x \mathcal{F}^{(k)}, \partial_x^2 \mathcal{F}^{(k)}, \partial_\theta \mathcal{F}^{(k)}, \partial_\theta^2 \mathcal{F}^{(k)}, \partial_{x\theta} \mathcal{F}^{(k)}$). Expressing the field equations in the residual form $\mathcal{R}(x, \theta, \partial \mathcal{F}^{(k)}) = 0$, and substituting the spectral expansions Eq. (19) into the residuals, we can calculate the resulting equations at Gauss-Chebyshev points defined by

$$x_l = \cos \left[\frac{(2l+1)\pi}{2N} \right], \quad \theta_m = \frac{(2m+1)\pi}{4N}, \quad l, m = 0, \dots, N-1. \quad (20)$$

Together with the boundary conditions, there are $N_{\mathcal{F}} \times N_x \times N_\theta$ algebraic equations for the spectral coefficients $\alpha_{ij}^{(k)}$, which is given by

$$\alpha_{ij}^{(k)} = \frac{4}{N_x N_\theta} \sum_{l=0}^{N_x-1} \sum_{m=0}^{N_\theta-1} \mathcal{F}^{(k)}(x_l, \theta_m) T_i(x_l) \cos(2j\theta_m). \quad (21)$$

To solve those algebraic equations with the Newton-Raphson iterative method, one has to provide an initial guess. Setting BH parameters, we expand the functions of the Kerr solution in the spectral series Eq.(19) to obtain the spectral coefficients $\alpha_{ij, Kerr}^{(k)}$. The values of coefficients $\alpha_{ij, Kerr}^{(k)}$ are set as initial guesses to the Newton solver to search for the spectral coefficients $\alpha_{ij}^{(k)}$ of the "potential" scalarized BH solution.

IV. NUMERICAL RESULTS

This section presents the numerical investigation of rotating scalarized BH solutions. Firstly, setting the parameter κ to different values, we show the spectrum of solutions.

A. The results for different κ

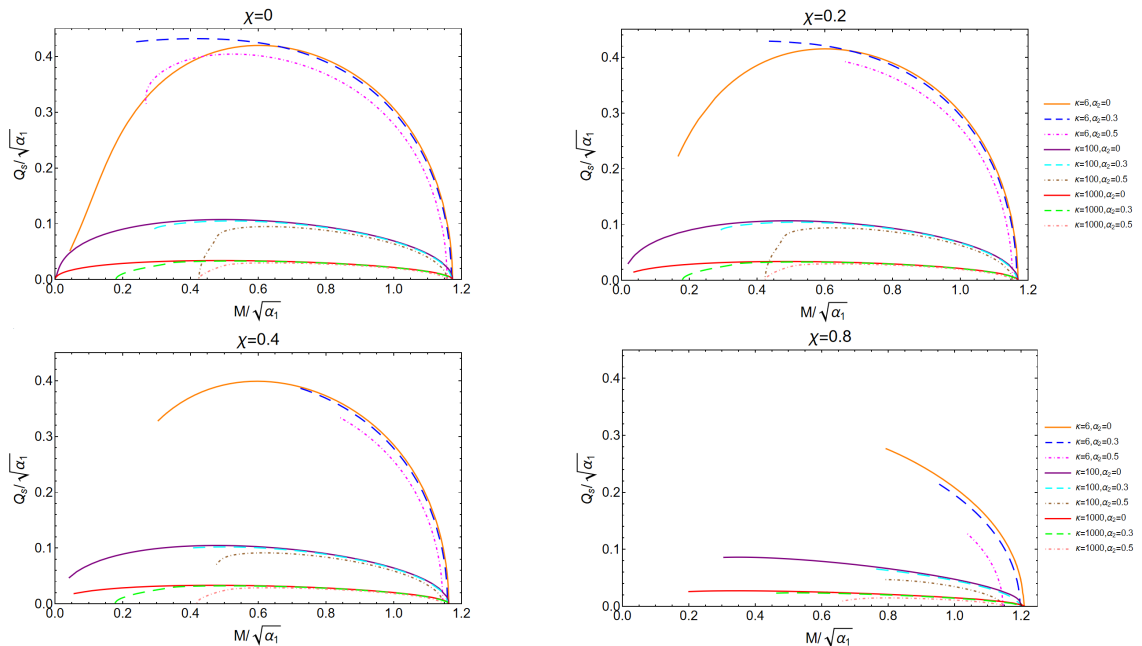


FIG. 1. Scalar charge $Q_s / \sqrt{\alpha_1}$ as a function of ADM mass $M / \sqrt{\alpha_1}$ for different parameters.

Fig. 1 presents the dimensionless scalar charge $Q_s / \sqrt{\alpha_1}$ as a function of the ADM mass $M / \sqrt{\alpha_1}$ for three different values of the parameter $\kappa = 6, 100, 1000$ and three coupling ratios $\alpha_2 / \alpha_1 = 0, 0.3, 0.5$. The four panels correspond to increasing values of the dimensionless spin parameter $\chi = 0$ (non-rotating), $\chi = 0.2, 0.4, 0.8$. Within each panel, the solution space is stratified into three distinct coupling regimes: the upper set corresponds to strong exponential coupling ($\kappa = 6$), the intermediate set to moderate coupling ($\kappa = 100$), and the lower set to weak coupling ($\kappa = 1000$). This hierarchical structure demonstrates an inverse relation between κ and the scalar charge $Q_s / \sqrt{\alpha_1}$, with the κ -dependent enhancement becoming more pronounced at higher spins. Moreover, for each curve, the left endpoint represents a critical set for the scalarized BH solution, while the right endpoint corresponds to an existence solution which is a marginal BH solution with zero scalar charge. These endpoints delineate the boundaries of the existence domain of the scalarized BHs, and they will be discussed in detail in the next section.

The comparative analysis of scalarized BH solutions across different coupling parameters reveals two key interdependent mechanisms governing their existence domains. First, the constant κ plays a decisive role in shaping the scalarization phase space through its inverse relationship with the magnitude of the scalar charge ($Q_s / \sqrt{\alpha_1}$). This is clearly reflected in the structure of the stratified solution, where the lower κ values correspond to upper-branch solutions with enhanced scalar charges. In addition, the quadratic coupling parameter α_2 systematically suppresses scalarization across all κ regimes. For fixed χ and κ , an increase in α_2 reduces both the scalar charge and the parametric range over which viable scalarized configurations exist. Second, rotational dynamics introduces a spin-dependent suppression mechanism. At fixed values of κ and α_2 , increasing the dimensionless spin χ from 0 to 0.8 reduces the existence domain of the solution. This spin suppression becomes particularly dominant at higher χ values. To isolate the α_2 - χ interaction while maintaining sufficient scalarization strength for accurate measurement, we focus on case $\kappa = 6$ for

a further detailed analysis of the properties of the solution in the following section.

B. The results for $\kappa = 6$

In this section, we present the domain of existence and the physical properties of rotating scalarized BHs with the coupling function $F(\phi) = (1 - e^{-6\phi^2})/6$.

Fixing the spin $\chi = 0$, Fig. 2 shows both the scalar charge and the entropy of the scalarized solution. In the no-rotating limit, the rotating scalarized solution reduces to the spherically symmetric cases, and consequently, Fig. 2 is identical to its counterpart in [63]. Each curve in the figure originates from an existence solution (right boundary point) and terminates at a critical solution (left boundary point). As shown in the right panel, the entropy of a scalarized BH exceeds that of a Schwarzschild BH with the same mass, with the exception of the coupling ratios $\alpha_2/\alpha_1 = 0.5$ and 0.7 at small masses. This observation indicates that scalarized BHs are entropically favored over Schwarzschild BHs in most cases. Furthermore, as the coupling ratio α_2/α_1 increases, the mass window for the scalarized BHs shrinks. Thus, we can conclude that the additional quadratic Gauss-Bonnet term suppresses the mass window for the scalarized BHs. In the following sections, we provide a more detailed discussion of the effect of the quartic Gauss-Bonnet term on rotating scalarized BHs.

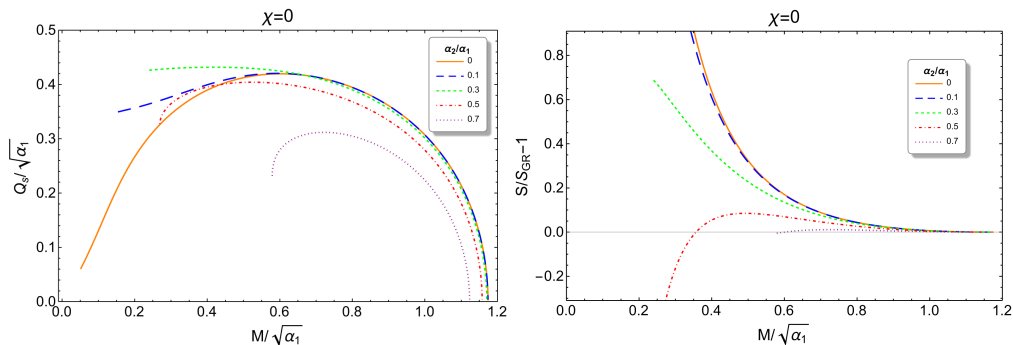


FIG. 2. Scalar charge $Q_s/\sqrt{\alpha_1}$ (left-hand panel) and entropy $S/S_{GR} - 1$ (right-hand panel) of the scalarized solutions as a function of $M/\sqrt{\alpha_1}$.

I. $\alpha_2/\alpha_1 = 0$

Turning off the coupling parameter α_2 , the left panel of Fig. 3 displays the existence domain of the scalarized BHs, while the right panel plots the entropy ratio $S/S_{GR} - 1$ as a function of the dimensionless spin χ . The existence domain (the darker shaded area) is bounded by three distinct sets of solutions: (1) the static spherically symmetric solutions labeled by dashed-dotted segment overlapping with the vertical axis where $\chi = 0$; (2) the existence line (solid blue line), which corresponds to the bifurcation edge from the Kerr family; and (3) the set of critical solutions marked by red regular triangles. Critical solutions are a common feature in sGB models [23, 76–79], and the numerical process fails to converge as the BH parameters approach the critical sets. This behavior can be explained by the fact that the quadratic equation of the second-order term

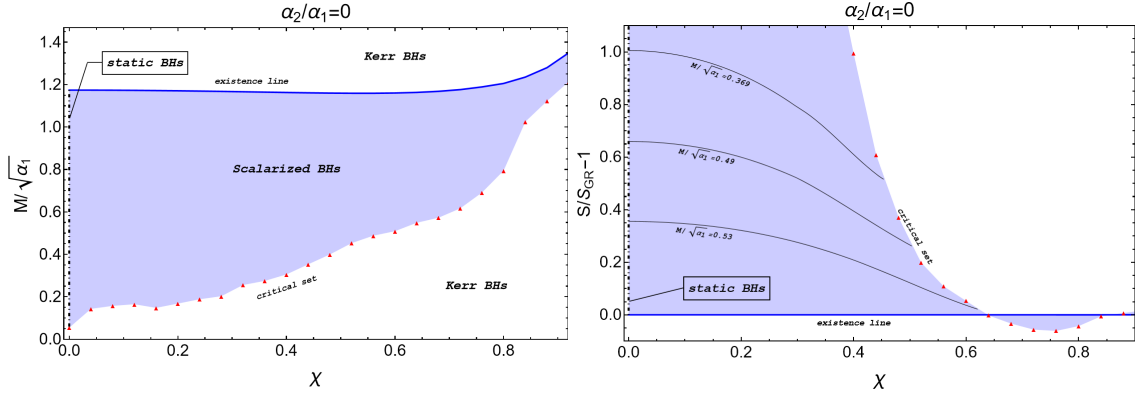


FIG. 3. The existence domain (left-hand panel), and entropy $S/S_{GR} - 1$ (right-hand panel) of scalarized BHs for the case with the coupling parameter $\alpha_2/\alpha_1 = 0$.

in the near-horizon expansion of the scalar field ceases to have a real solution as the critical set is approached. Accordingly, a uniform near-horizon expansion of the solution is no longer feasible, demonstrating that there does not exist a regular solution; for further details, see [23, 80]. Note that the static spherically symmetric solutions correspond to the solid orange curve in Fig. 2. Furthermore, the right panel compares the entropy S of scalarized BHs with that of Kerr holes, S_{GR} , having the same mass and spin. The comparison shows that, for $\chi < 0.64$, most scalarized solutions are thermodynamically more stable than their Kerr counterpart.

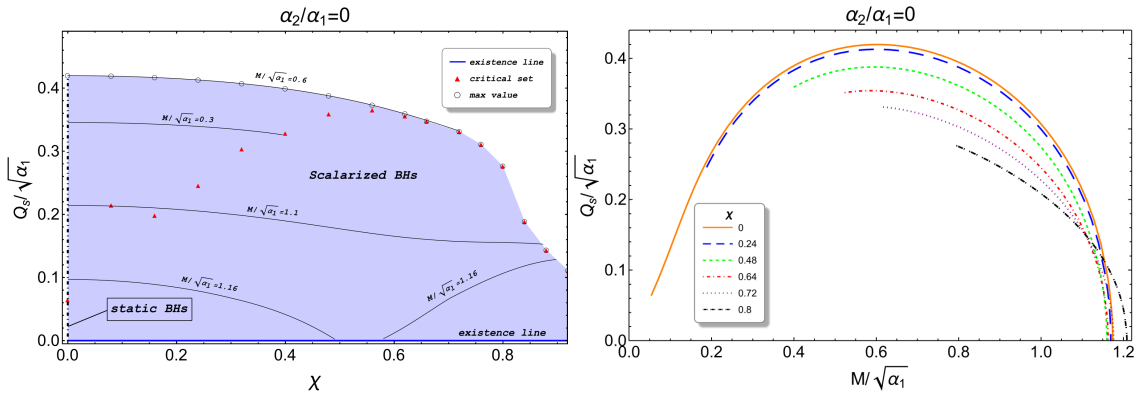


FIG. 4. Setting $\alpha_2/\alpha_1 = 0$, the left panel shows scalar charge $Q_s/\sqrt{\alpha_1}$ of the scalarized solutions versus spin χ , while the right panel gives scalar charge $Q_s/\sqrt{\alpha_1}$ versus ADM mass $M/\sqrt{\alpha_1}$.

To show the strength of the scalar field, Fig. 4 illustrates the scalar charge $Q_s/\sqrt{\alpha_1}$ of scalarized BHs as a function of their mass and dimensionless spin. In the left panel, for spins $\chi < 0.72$, the scalar charge at the critical set does not coincide with the maximum values (labeled by the empty circles) that form the upper boundary. As the dimensionless spin $\chi \geq 0.72$, the critical sets coincide with the upper boundary. To further examine the dependence of the scalar charge on both BH mass and spin, the right panel displays plots of $Q_s/\sqrt{\alpha_1}$ versus $M/\sqrt{\alpha_1}$ for various values of χ . In these curves, the left endpoint represents a critical solution (marked by a red regular triangle in the left panel), while the right endpoint corresponds to an existence solution (denoted by the solid blue line). As shown, for spins $\chi < 0.72$, the scalar charge initially increases with mass, reaches a maximum, and then decreases, resulting in a parabolic distribution. As χ increases,

the curves become monotonic, with the maximum scalar charge occurring at the critical solution. This behavior indicates that only for sufficiently large values of $\chi(\geq 0.72)$ do the scalar charge of critical solutions coincide with the maximum scalar charge.

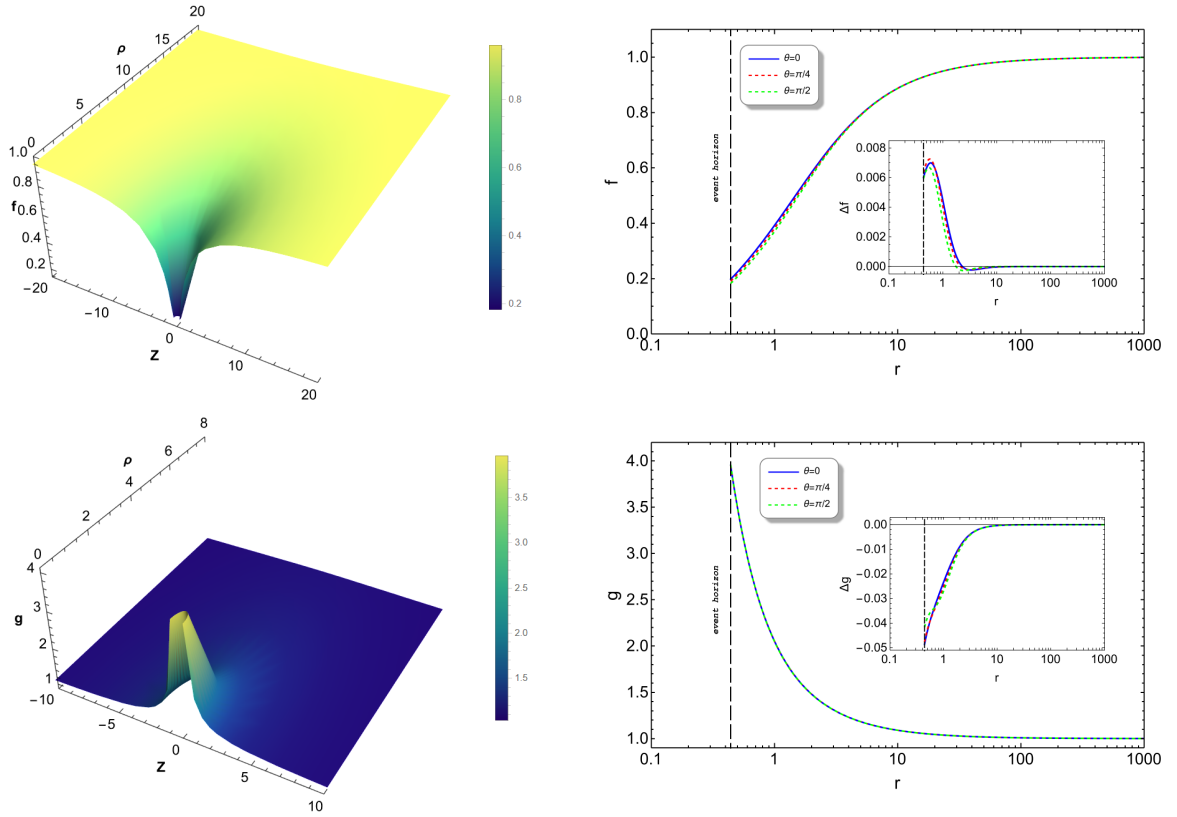


FIG. 5. Metric functions f and g for scalarized rotating BH solution with the parameters $\chi = 0.5$, $r_H = 0.44$ (dashed black line) and $\alpha_2 = 0$. The deviations between the scalarized BH and the Kerr BH are described by $\Delta f = f - f_{Kerr}$ and $\Delta g = g - g_{Kerr}$.

Using the parameters $\chi = 0.5$, $r_H = 0.44$, we obtained a numerical solution with the BH mass $M = 1.04724$ and the scalar charge $Q_s = 0.234718$. Figs. 5 and 6 present the corresponding metric function and scalar fields. In these figures, the left columns display three-dimensional (3D) plots, while the right columns show two-dimensional (2D) plots of the functions as a function of the radial variable for three different angular values. For the 3D plots, the axes are defined by $\rho = r \sin \theta$ and $Z = r \cos \theta$ (with $r \geq r_H$). Additionally, we depict the deviations between the scalarized rotating BH and the Kerr BH with the same χ and r_H in these figures. From Figs. 5 and 6, one can see that our numerical solutions exhibit smooth profiles, which leads to finite curvature invariants in the full domain of integration, and our scalarized rotating BH solution is asymptotically flat and has scalar hair.

2. $\alpha_2/\alpha_1 = 0.3$

To disclose the impact of additional term \mathcal{G}^2 on scalarization, we set the coupling parameter to be $\alpha_2/\alpha_1 = 0.3$ without loss of generality. In the left panel of Fig. 7, we give the existence

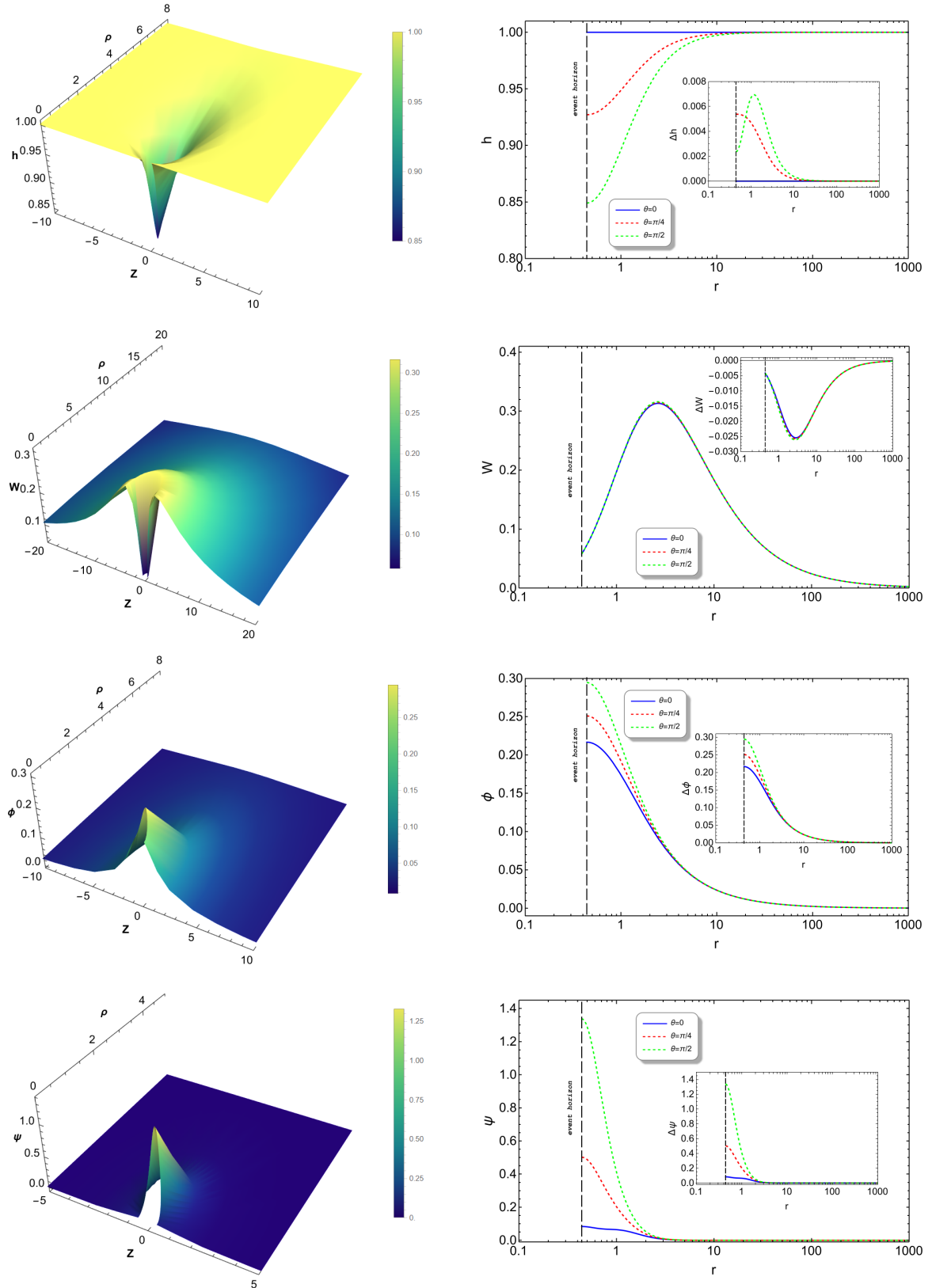


FIG. 6. Metric functions h , W and scalar fields for scalarized rotating BH solution with the same parameters as in Fig. 5. The deviations between the scalarized BH and the Kerr BH are described by $\Delta h = h - h_{Kerr}$ and $\Delta W = W - W_{Kerr}$.

domain of scalarized BHs, parametrized by mass $M/\sqrt{\alpha_1}$ and dimensionless spin χ . The domain of scalarized BHs (darker shaded area) is bounded by three sets of solutions: the static BHs (dash-dotted line), the existence line (solid blue line), and the critical sets (red regular triangles). The static solutions here correspond to the green dished curve in Fig. 2. Comparing Fig. 7 with Fig. 3, we see that the region of scalarized BHs becomes compressed as α_2 increases, and the scalarization is suppressed for lower massive BHs. We also calculated the entropy S of the scalarized BHs, and compared it with that of Kerr BHs S_{GR} with the same mass and spin. The right panel of Fig. 7 displays the relative entropy $S/S_{GR} - 1$. In the region where $\chi \lesssim 0.55$, we find that $S/S_{GR} - 1 > 0$, indicating that scalarized solutions are more favored by thermodynamics.

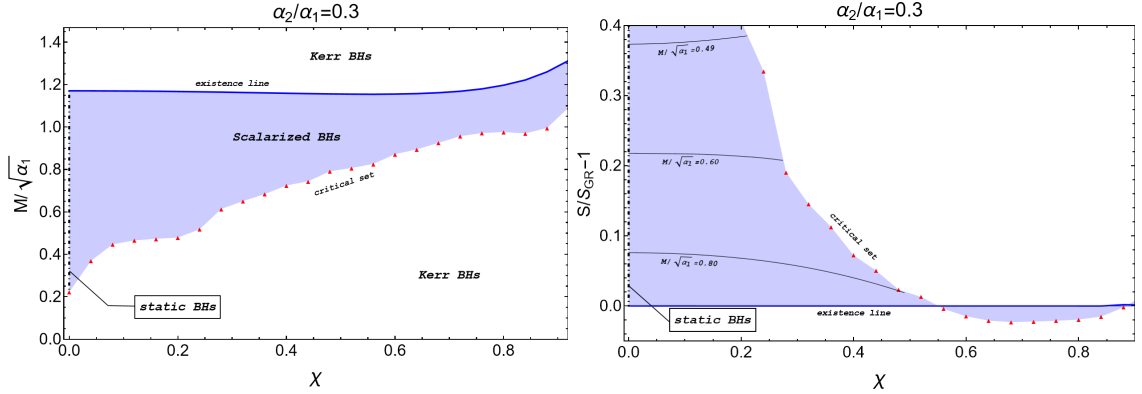


FIG. 7. ADM mass $M/\sqrt{\alpha_1}$ (left-hand panel) and entropy $S/S_{GR} - 1$ (right-hand panel) as functions of dimensionless spin χ with the coupling parameters $\alpha_2/\alpha_1 = 0.3$.

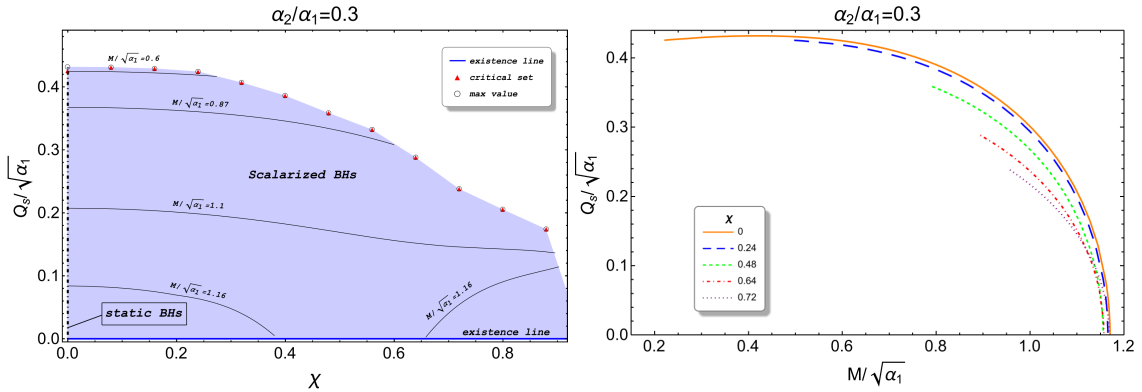


FIG. 8. Scalar charge $Q_s/\sqrt{\alpha_1}$ of the scalarized solutions versus χ (left panel), and versus $M/\sqrt{\alpha_1}$ (right panel).

Fig. 8 illustrates how the scalar charge varies with BH mass and spin. In the left panel, the dashed-dotted line corresponds to the orange solid line in the right panel, and it also matches the green dashed curve in the left panel of Fig. 2. For BHs with $\chi < 0.08$, the scalar charge of critical solutions (marked by empty circles) serves as the upper bound; however, in the low-spin regime $\chi < 0.08$, the maximum scalar charge shifts from critical solutions to intermediate parametric regions. In the right panel, all the curves originate from critical solutions and terminate at existence solutions (characterized by a vanishing scalar charge $Q_s/\sqrt{\alpha_1} = 0$). The curve with $\chi < 0.08$

follow parabolic behavior, whereas those for $\chi \geq 0.08$ follow monotonic shapes. Comparing Fig. 8 with Fig. 4, we find that the region of scalarized BHs reduces when the coupling ratio α_2/α_1 increases. This finding indicates that the additional term \mathcal{G}^2 exerts an inhibitory effect on scalarization.

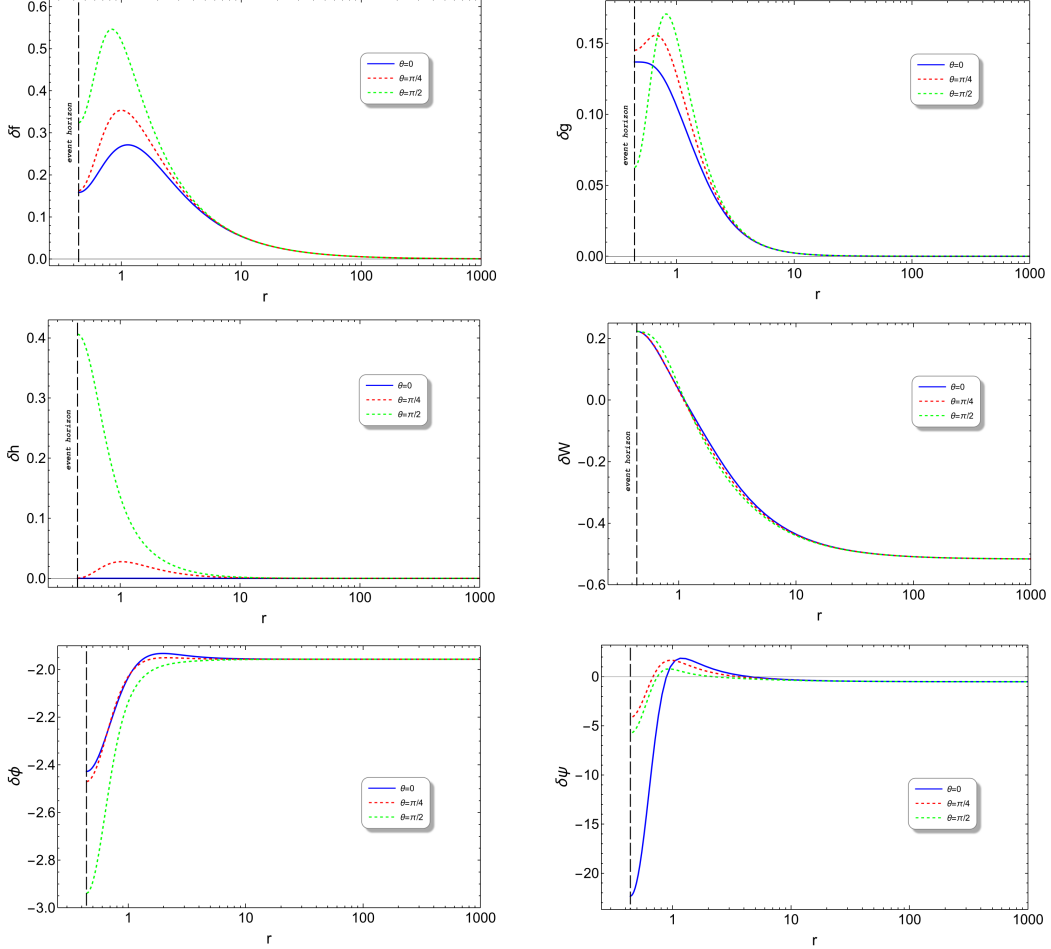


FIG. 9. Comparison of the metric functions f, g, h, W and the scalar fields ϕ and ψ for the scalarized rotating BH solutions with coupling ratio $\alpha_2/\alpha_1 = 0$ and $\alpha_2/\alpha_1 = 0.3$, using the same parameters as Fig. 5.

To assess the impact of the quartic term \mathcal{G}^2 on the spacetime geometry and scalar fields, we calculate numerical solutions for the model with $\alpha_2/\alpha_1 = 0.3$ and compare them with those obtained with $\alpha_2/\alpha_1 = 0$. Using the same BH parameters $r_H = 0.44$ and $\chi = 0.5$ as in Figs. 5 and 6, we obtain an ADM mass $M = 1.04453$ and a scalar charge of $Q_s = 0.230125$. To quantitatively describe the difference, we define the percentage change for each function as $\delta\mathcal{F}^{(k)} = (\mathcal{F}_{\alpha_2=0.3}^{(k)} - \mathcal{F}_{\alpha_2=0}^{(k)})/\mathcal{F}_{\alpha_2=0}^{(k)} \times 100$ with $\mathcal{F}^{(k)} = \{f, g, h, W, \phi, \psi\}$. Fig. 9 shows the numerical results for $\delta\mathcal{F}^{(k)}$. We observe that, except for Ψ , the functions $\mathcal{F}^{(k)}$ exhibit only minor deviations from those in the case $\alpha_2/\alpha_1 = 0$. The percentage change for the metric functions is of the order of 0.1%, while for the scalar field ϕ , the maximum deviation is approximately 3% near the horizon. In contrast, the scalar field $\Psi = \mathcal{G}$ shows a more pronounced difference, with deviations reaching around 20% near the horizon. This larger discrepancy arises because, although the scalar functions themselves differ only slightly, their second-order derivatives with respect to r have significant fluctuations

near the horizon. These fluctuations amplify the variation in Ψ , resulting in the observed difference. For example, Fig.10 gives the percentage change in the derivatives of the metric function f .

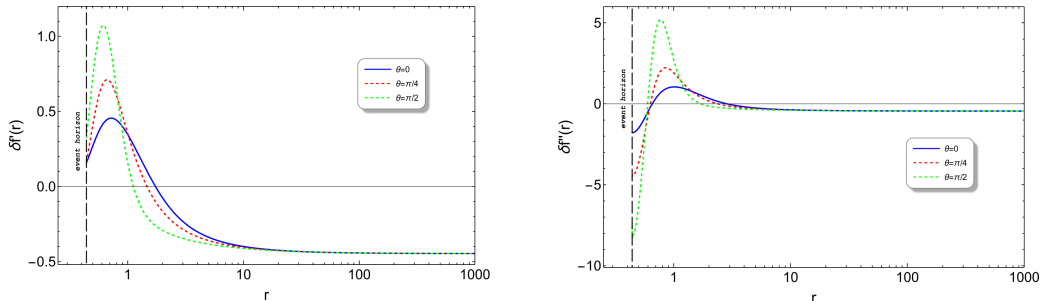


FIG. 10. The percentage change of the first order derivative (left panel) and second order derivative (right panel) of metric function f .

V. CONCLUSIONS

In this study, we explored how rotating BHs behave in the context of a class of sGB gravity theories that incorporate a quadratic Gauss-Bonnet term. We focus on three key factors: (1) the constant κ , which corresponds to the coupling strength between the gravitational field and scalar field; (2) the dimensionless spin parameter (χ), which measures how fast a BH rotates, (3) and the coupling constant (α_2), which represents additional gravitational effects in sGB gravity. Our goal is to understand how these factors influence the existence and properties of scalarized BHs. By numerically solving the field equations under stationary and axisymmetric conditions, we demonstrated that the constant κ plays a critical role in shaping the characteristics of scalarized BHs in sGB gravity. Smaller κ values enhance the coupling strength, leading to larger scalar charges. Moreover, we demonstrated that the scalarization of BHs is significantly suppressed by the spin parameter (χ) and the quadratic coupling constant (α_2). Specifically, increasing α_2 narrows the domain of existence for scalarized solutions, particularly for lower-mass BHs. This suppression arises from the \mathcal{G}^2 -term in the effective mass m_{eff}^2 , which stabilizes general relativity solutions against tachyonic instabilities.

Furthermore, scalarized BHs are shown to be thermodynamically favored over Kerr BHs with identical mass and spin in most parameter regimes, as evidenced by their higher entropy ($S/S_{GR} > 1$). However, this entropic preference diminished for highly spinning BHs or large α_2 . These results challenge the "Kerr hypothesis" and highlight the role of modified gravity in enriching the BH phase space. The predicted scalarization mass windows could be probed by future gravitational wave detectors like LISA, Taiji and TianQin, offering observational constraints on the coupling constants α_1 and α_2 . Future work should focus on dynamical scenarios, such as BH mergers or accretion processes, to validate these predictions and refine the parameter space of sGB gravity.

ACKNOWLEDGMENTS

This research is supported by the National Natural Science Foundation of China under Grant Nos.12375056, 12375048, and the Postgraduate Research & Practice Innovation Program of Jiangsu Province under Grant No.KYCX223452. Some of our calculations were performed using the tensor-algebra bundle xAct [81].

APPENDIX: RESOLUTION SETTINGS FOR COMPUTATION

In this appendix, we provide an example to explain why we constructed a grid with $N_x = 40$ and $N_\theta = 8$ when using Chebyshev pseudo-spectral and Newton-Raphson methods to solve the system of field equations in this paper.

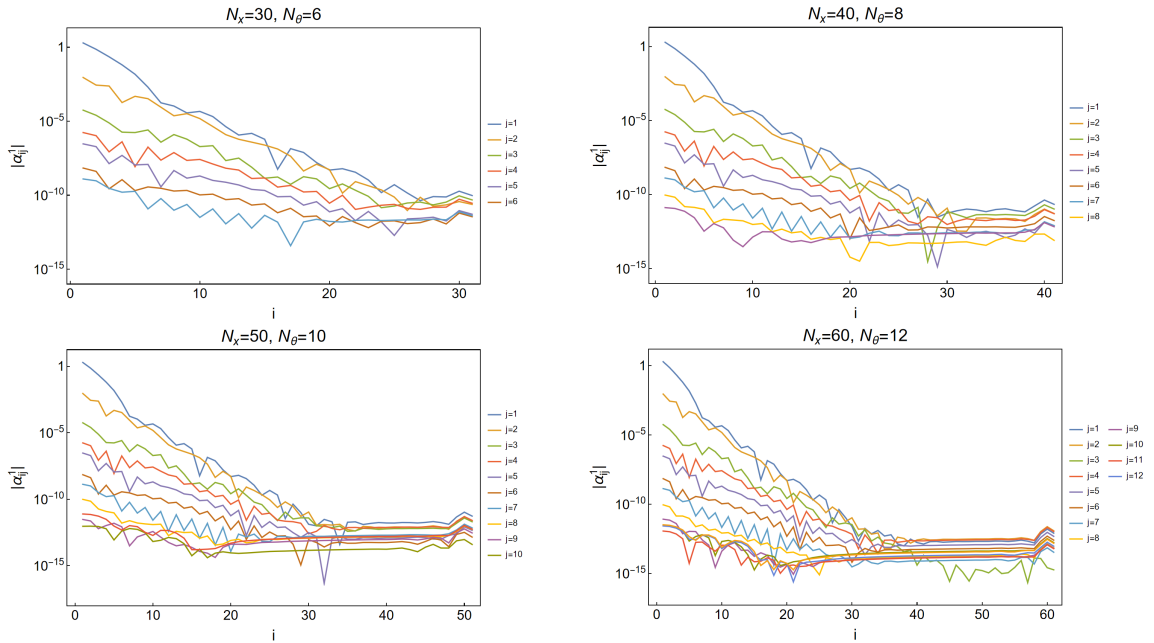


FIG. 11. The absolute values of the spectral decomposition coefficients $\alpha_{ij}^{(1)}$ of the metric function $f(x, \theta)$ with different (N_x, N_θ) .

Employing the dimensionless parameters $r_H = 0.46$ (horizon radius) and dimensionless spin $\chi = 0.4$, we present in Fig. 11 the spectral decomposition coefficients $\alpha_{ij}^{(1)}$ (see Eq.(19)) governing the metric function $f(x, \theta)$. One can see from it that the magnitudes $|\alpha_{ij}^{(1)}|$ exhibit an exponential decay with increasing index values of i for each j , which demonstrates the convergent characteristic of numerical scheme. Consequently, the functional value $f(x, \theta)$ predominantly depends on the leading terms in the $\alpha_{ij}^{(1)}$ series. Even when the values of (N_x, N_θ) increase from $(40, 8)$ to $(50, 10)$ and $(60, 12)$, the original coefficients remain unchanged, and the additional coefficients become negligible. Moreover, if set $N_x = 30$ and $N_\theta = 6$, we are not sure that those leading terms could approximate the true scalarized BH solution. Through a comprehensive evaluation of computational efficiency and numerical accuracy, $N_x = 40$ and $N_\theta = 8$ have been identified as the optimal

configurations for main computations in this work.

- [1] Piotr T Chruściel, João Lopes Costa, and Markus Heusler. Stationary black holes: uniqueness and beyond. *Living Reviews in Relativity*, 15:1–73, 2012.
- [2] R.P. Kerr. The Kerr spacetime: rotating black holes in general relativity, 2009.
- [3] D. C. Robinson. Uniqueness of the Kerr Black Hole. *Phys. Rev. Lett.*, 34:905–906, Apr 1975.
- [4] B. Carter. Axisymmetric Black Hole Has Only Two Degrees of Freedom. *Phys. Rev. Lett.*, 26:331–333, Feb 1971.
- [5] Carlos A. R. Herdeiro and Eugen Radu. Asymptotically flat black holes with scalar hair: A review. *International Journal of Modern Physics D*, 24(09):1542014, 2015.
- [6] Carlos A. R. Herdeiro. Black Holes: On the Universality of the Kerr Hypothesis. In Christian Pfeifer and Claus Lämmerzahl, editors, *Modified and Quantum Gravity: From Theory to Experimental Searches on All Scales*, pages 315–331. Springer International Publishing, Cham, 2023.
- [7] Paolo Pani, Caio F. B. Macedo, Luis C. B. Crispino, and Vitor Cardoso. Slowly rotating black holes in alternative theories of gravity. *Phys. Rev. D*, 84:087501, 2011.
- [8] Carlos A. R. Herdeiro and Eugen Radu. Kerr black holes with scalar hair. *Phys. Rev. Lett.*, 112:221101, 2014.
- [9] Eugeny Babichev and Christos Charmousis. Dressing a black hole with a time-dependent Galileon. *JHEP*, 08:106, 2014.
- [10] Mariano Cadoni, Giuseppe D’Appollonio, and Paolo Pani. Phase transitions between Reissner-Nordstrom and dilatonic black holes in 4D AdS spacetime. *JHEP*, 03:100, 2010.
- [11] Vitor Cardoso, Isabella P. Carucci, Paolo Pani, and Thomas P. Sotiriou. Black holes with surrounding matter in scalar-tensor theories. *Phys. Rev. Lett.*, 111:111101, 2013.
- [12] Burkhard Kleihaus, Jutta Kunz, and Stoytcho Yazadjiev. Scalarized Hairy Black Holes. *Phys. Lett. B*, 744:406–412, 2015.
- [13] Hector O. Silva, Caio F. B. Macedo, Thomas P. Sotiriou, Leonardo Gualtieri, Jeremy Sakstein, and Emanuele Berti. Stability of scalarized black hole solutions in scalar-Gauss-Bonnet gravity. *Phys. Rev. D*, 99(6):064011, 2019.
- [14] M. S. Volkov and D. V. Galtsov. NonAbelian Einstein Yang-Mills black holes. *JETP Lett.*, 50:346–350, 1989.

- [15] P. Bizon. Colored black holes. *Phys. Rev. Lett.*, 64:2844–2847, 1990.
- [16] Brian R. Greene, Samir D. Mathur, and Christopher M. O’Neill. Eluding the no hair conjecture: Black holes in spontaneously broken gauge theories. *Phys. Rev. D*, 47:2242–2259, 1993.
- [17] Kei-Ichi Maeda, T. Tachizawa, T. Torii, and T. Maki. Stability of nonAbelian black holes and catastrophe theory. *Phys. Rev. Lett.*, 72:450–453, 1994.
- [18] Hugh Luckcock and Ian Moss. BLACK HOLES HAVE SKYRMION HAIR. *Phys. Lett. B*, 176:341–345, 1986.
- [19] Serge Droz, Markus Heusler, and Norbert Straumann. New black hole solutions with hair. *Phys. Lett. B*, 268:371–376, 1991.
- [20] J. D. Bekenstein. Exact solutions of Einstein conformal scalar equations. *Annals Phys.*, 82:535–547, 1974.
- [21] Takashi Torii, Hiroki Yajima, and Kei-ichi Maeda. Dilatonic black holes with Gauss-Bonnet term. *Phys. Rev. D*, 55:739–753, 1997.
- [22] P. Kanti and K. Tamvakis. Colored black holes in higher curvature string gravity. *Phys. Lett. B*, 392:30–38, 1997.
- [23] Burkhard Kleihaus, Jutta Kunz, Sindy Mojica, and Eugen Radu. Spinning black holes in Einstein–Gauss-Bonnet–dilaton theory: Nonperturbative solutions. *Phys. Rev. D*, 93:044047, Feb 2016.
- [24] Burkhard Kleihaus, Jutta Kunz, and Eugen Radu. Rotating Black Holes in Dilatonic Einstein-Gauss-Bonnet Theory. *Phys. Rev. Lett.*, 106:151104, 2011.
- [25] Zong-Kuan Guo, Nobuyoshi Ohta, and Takashi Torii. Black Holes in the Dilatonic Einstein-Gauss-Bonnet Theory in Various Dimensions. I. Asymptotically Flat Black Holes. *Prog. Theor. Phys.*, 120:581–607, 2008.
- [26] Dimitry Ayzenberg and Nicolas Yunes. Slowly-Rotating Black Holes in Einstein-Dilaton-Gauss-Bonnet Gravity: Quadratic Order in Spin Solutions. *Phys. Rev. D*, 90:044066, 2014. [Erratum: *Phys.Rev.D* 91, 069905 (2015)].
- [27] Kei-ichi Maeda, Nobuyoshi Ohta, and Yukinori Sasagawa. Black Hole Solutions in String Theory with Gauss-Bonnet Curvature Correction. *Phys. Rev. D*, 80:104032, 2009.
- [28] Nobuyoshi Ohta and Takashi Torii. Global Structure of Black Holes in String Theory with Gauss-Bonnet Correction in Various Dimensions. *Prog. Theor. Phys.*, 124:207–225, 2010.
- [29] Thomas P. Sotiriou and Shuang-Yong Zhou. Black hole hair in generalized scalar-tensor gravity: An explicit example. *Phys. Rev. D*, 90:124063, 2014.

- [30] Robert Benkel, Thomas P. Sotiriou, and Helvi Witek. Black hole hair formation in shift-symmetric generalised scalar-tensor gravity. *Class. Quant. Grav.*, 34(6):064001, 2017.
- [31] Georgios Antoniou, Antoine Lehébel, Giulia Ventagli, and Thomas P. Sotiriou. Black hole scalarization with Gauss-Bonnet and Ricci scalar couplings. *Phys. Rev. D*, 104(4):044002, 2021.
- [32] Yunqi Liu, Cheng-Yong Zhang, Wei-Liang Qian, Kai Lin, and Bin Wang. Dynamic generation or removal of a scalar hair. *JHEP*, 01:074, 2023.
- [33] Jia-Yan Jiang, Qian Chen, Yunqi Liu, Yu Tian, Wei Xiong, Cheng-Yong Zhang, and Bin Wang. Type I critical dynamical scalarization and descalarization in Einstein-Maxwell-scalar theory. *Sci. China Phys. Mech. Astron.*, 67(2):220411, 2024.
- [34] Cheng-Yong Zhang, Qian Chen, Yunqi Liu, Wen-Kun Luo, Yu Tian, and Bin Wang. Dynamical transitions in scalarization and descalarization through black hole accretion. *Phys. Rev. D*, 106(6):L061501, 2022.
- [35] Daniela D. Doneva, Lucas G. Collodel, and Stoytcho S. Yazadjiev. Spontaneous nonlinear scalarization of Kerr black holes. *Phys. Rev. D*, 106(10):104027, 2022.
- [36] Daniela D. Doneva, Fethi M. Ramazanoğlu, Hector O. Silva, Thomas P. Sotiriou, and Stoytcho S. Yazadjiev. Spontaneous scalarization. *Rev. Mod. Phys.*, 96(1):015004, 2024.
- [37] Daniela D. Doneva, Christian J. Krüger, Kalin V. Staykov, and Petar Y. Yordanov. Neutron stars in Gauss-Bonnet gravity: Nonlinear scalarization and gravitational phase transitions. *Phys. Rev. D*, 108(4):044054, 2023.
- [38] Yunqi Liu, Cheng-Yong Zhang, Qian Chen, Zhoujian Cao, Yu Tian, and Bin Wang. Critical scalarization and descalarization of black holes in a generalized scalar-tensor theory. *Sci. China Phys. Mech. Astron.*, 66(10):100412, 2023.
- [39] Shao-Jun Zhang. Nonlinear instability and scalar clouds of spherical exotic compact objects in scalar-Gauss-Bonnet theory. *Eur. Phys. J. C*, 83(10):950, 2023.
- [40] Meng-Yun Lai, De-Cheng Zou, Rui-Hong Yue, and Yun Soo Myung. Nonlinearly scalarized rotating black holes in Einstein-scalar-Gauss-Bonnet theory. *Phys. Rev. D*, 108(8):084007, 2023.
- [41] Masato Minamitsuji and Shinji Mukohyama. Instability of scalarized compact objects in Einstein-scalar-Gauss-Bonnet theories. *Phys. Rev. D*, 108(2):024029, 2023.
- [42] Thibault Damour and Gilles Esposito-Farese. Nonperturbative strong field effects in tensor - scalar theories of gravitation. *Phys. Rev. Lett.*, 70:2220–2223, 1993.
- [43] Vitor Cardoso, Isabella P. Carucci, Paolo Pani, and Thomas P. Sotiriou. Matter around Kerr black

- holes in scalar-tensor theories: scalarization and superradiant instability. *Phys. Rev. D*, 88:044056, 2013.
- [44] Cheng-Yong Zhang, Shao-Jun Zhang, and Bin Wang. Superradiant instability of Kerr-de Sitter black holes in scalar-tensor theory. *JHEP*, 08:011, 2014.
- [45] Daniela D. Doneva and Stoytcho S. Yazadjiev. New Gauss-Bonnet Black Holes with Curvature-Induced Scalarization in Extended Scalar-Tensor Theories. *Phys. Rev. Lett.*, 120(13):131103, 2018.
- [46] Hector O. Silva, Jeremy Sakstein, Leonardo Gualtieri, Thomas P. Sotiriou, and Emanuele Berti. Spontaneous scalarization of black holes and compact stars from a Gauss-Bonnet coupling. *Phys. Rev. Lett.*, 120(13):131104, 2018.
- [47] G. Antoniou, A. Bakopoulos, and P. Kanti. Evasion of No-Hair Theorems and Novel Black-Hole Solutions in Gauss-Bonnet Theories. *Phys. Rev. Lett.*, 120(13):131102, 2018.
- [48] Pedro V. P. Cunha, Carlos A. R. Herdeiro, and Eugen Radu. Spontaneously Scalarized Kerr Black Holes in Extended Scalar-Tensor–Gauss-Bonnet Gravity. *Phys. Rev. Lett.*, 123(1):011101, 2019.
- [49] Alexandru Dima, Enrico Barausse, Nicola Franchini, and Thomas P. Sotiriou. Spin-induced black hole spontaneous scalarization. *Phys. Rev. Lett.*, 125(23):231101, 2020.
- [50] Carlos A. R. Herdeiro, Eugen Radu, Hector O. Silva, Thomas P. Sotiriou, and Nicolás Yunes. Spin-induced scalarized black holes. *Phys. Rev. Lett.*, 126(1):011103, 2021.
- [51] Emanuele Berti, Lucas G. Collodel, Burkhard Kleihaus, and Jutta Kunz. Spin-induced black-hole scalarization in Einstein-scalar-Gauss-Bonnet theory. *Phys. Rev. Lett.*, 126(1):011104, 2021.
- [52] Fabrizio Corelli, Marina De Amicis, Taishi Ikeda, and Paolo Pani. What is the Fate of Hawking Evaporation in Gravity Theories with Higher Curvature Terms? *Phys. Rev. Lett.*, 130(9):091501, 2023.
- [53] Fabrizio Corelli, Marina De Amicis, Taishi Ikeda, and Paolo Pani. Nonperturbative gedanken experiments in Einstein-dilaton-Gauss-Bonnet gravity: Nonlinear transitions and tests of the cosmic censorship beyond general relativity. *Phys. Rev. D*, 107(4):044061, 2023.
- [54] Carlos A. R. Herdeiro and Eugen Radu. Black hole scalarization from the breakdown of scale invariance. *Phys. Rev. D*, 99(8):084039, 2019.
- [55] Yves Brihaye, Carlos Herdeiro, and Eugen Radu. The scalarised Schwarzschild-NUT spacetime. *Phys. Lett. B*, 788:295–301, 2019.
- [56] Carlos A. R. Herdeiro, Eugen Radu, Nicolas Sanchis-Gual, and José A. Font. Spontaneous Scalarization of Charged Black Holes. *Phys. Rev. Lett.*, 121(10):101102, 2018.

- [57] Cheng-Yong Zhang, Peng Liu, Yunqi Liu, Chao Niu, and Bin Wang. Evolution of anti-de Sitter black holes in Einstein-Maxwell-dilaton theory. *Phys. Rev. D*, 105(2):024010, 2022.
- [58] Daniela D. Doneva and Stoytcho S. Yazadjiev. Beyond the spontaneous scalarization: New fully nonlinear mechanism for the formation of scalarized black holes and its dynamical development. *Phys. Rev. D*, 105(4):L041502, 2022.
- [59] Jose Luis Blázquez-Salcedo, Daniela D. Doneva, Jutta Kunz, and Stoytcho S. Yazadjiev. Radial perturbations of scalar-Gauss-Bonnet black holes beyond spontaneous scalarization. *Phys. Rev. D*, 105(12):124005, 2022.
- [60] Cheng-Yong Zhang, Qian Chen, Yunqi Liu, Wen-Kun Luo, Yu Tian, and Bin Wang. Critical Phenomena in Dynamical Scalarization of Charged Black Holes. *Phys. Rev. Lett.*, 128(16):161105, 2022.
- [61] Chao-Ming Zhang, Zhen-Hao Yang, Meng-Yun Lai, Yun Soo Myung, and De-Cheng Zou. Nonlinear scalarization of Schwarzschild black holes in Einstein-scalar-Gauss-Bonnet gravity. 4 2024.
- [62] P. A. González, Eleftherios Papantonopoulos, Joaquín Robledo, and Yerko Vásquez. Nonlinear scalarization of Schwarzschild black holes in scalar-torsion teleparallel gravity. *Phys. Rev. D*, 111(4):044064, 2025.
- [63] Astrid Eichhorn, Pedro GS Fernandes, Aaron Held, and Hector O Silva. Breaking black-hole uniqueness at supermassive scales. *arXiv preprint arXiv:2312.11430*, 2023.
- [64] K. Danzmann. LISA: An ESA cornerstone mission for a gravitational wave observatory. *Class. Quant. Grav.*, 14:1399–1404, 1997.
- [65] Wen-Rui Hu and Yue-Liang Wu. The Taiji Program in Space for gravitational wave physics and the nature of gravity. *Natl. Sci. Rev.*, 4(5):685–686, 2017.
- [66] Jun Luo et al. TianQin: a space-borne gravitational wave detector. *Class. Quant. Grav.*, 33(3):035010, 2016.
- [67] En-Kun Li et al. Gravitational Wave Astronomy With TianQin. 9 2024.
- [68] Alexandru Dima, Enrico Barausse, Nicola Franchini, and Thomas P. Sotiriou. Spin-Induced Black Hole Spontaneous Scalarization. *Phys. Rev. Lett.*, 125:231101, Dec 2020.
- [69] Shahar Hod. Onset of spontaneous scalarization in spinning Gauss-Bonnet black holes. *Phys. Rev. D*, 102:084060, Oct 2020.
- [70] Shao-Jun Zhang, Bin Wang, Anzhong Wang, and Joel F. Saavedra. Object picture of scalar field perturbation on Kerr black hole in scalar-Einstein-Gauss-Bonnet theory. *Phys. Rev. D*, 102:124056, Dec 2020.

- [71] Daniela D. Doneva, Lucas G. Collodel, Christian J. Krüger, and Stoytcho S. Yazadjiev. Black hole scalarization induced by the spin: $2 + 1$ time evolution. *Phys. Rev. D*, 102:104027, Nov 2020.
- [72] Hector O. Silva, Jeremy Sakstein, Leonardo Gualtieri, Thomas P. Sotiriou, and Emanuele Berti. Spontaneous Scalarization of Black Holes and Compact Stars from a Gauss-Bonnet Coupling. *Phys. Rev. Lett.*, 120:131104, Mar 2018.
- [73] Pedro GS Fernandes and David J Mulryne. A new approach and code for spinning black holes in modified gravity. *Classical and Quantum Gravity*, 40(16):165001, 2023.
- [74] Robert M Wald. Black hole entropy is the Noether charge. *Physical Review D*, 48(8):R3427, 1993.
- [75] Vivek Iyer and Robert M Wald. Some properties of the Noether charge and a proposal for dynamical black hole entropy. *Physical review D*, 50(2):846, 1994.
- [76] Thomas P. Sotiriou and Shuang-Yong Zhou. Black hole hair in generalized scalar-tensor gravity: An explicit example. *Phys. Rev. D*, 90:124063, Dec 2014.
- [77] P. Kanti, N. E. Mavromatos, J. Rizos, K. Tamvakis, and E. Winstanley. Dilatonic black holes in higher curvature string gravity. *Phys. Rev. D*, 54:5049–5058, Oct 1996.
- [78] Thomas P. Sotiriou and Shuang-Yong Zhou. Black Hole Hair in Generalized Scalar-Tensor Gravity. *Phys. Rev. Lett.*, 112:251102, Jun 2014.
- [79] Burkhard Kleihaus, Jutta Kunz, and Eugen Radu. Rotating Black Holes in Dilatonic Einstein-Gauss-Bonnet Theory. *Phys. Rev. Lett.*, 106:151104, Apr 2011.
- [80] Jorge FM Delgado, Carlos AR Herdeiro, and Eugen Radu. Spinning black holes in shift-symmetric Horndeski theory. *Journal of High Energy Physics*, 2020(4):1–32, 2020.
- [81] xAct: Efficient tensor computer algebra for the Wolfram Language. <http://www.xact.es/>.